Journal of
Synchrotron Radiation

ISSN 0909-0495

Received 13 June 2006
Accepted 1 August 2006

X-ray intensity fluctuation spectroscopy by heterodyne detection

F. Livet,[a]* F. Bley,[a] F. Ehrburger-Dolle,[b] I. Morfin,[b] E. Geissler[b] and M. Sutton[c]

[a]LTPCM-ENSEEG, UMR-CNRS 5614, INPG/UJF, BP 75, 38402 St Martin d'Hères, France, [b]LSP, UMR CNRS 5588 UJF, BP 87, 38402 St Martin d'Hères CEDEX, France, and [c]Physics Department, McGill University, Montreal, Québec, Canada H3A 2T8. E-mail: flivet@ltpcm.inpg.fr

A straightforward way of measuring X-ray intensity fluctuation spectroscopy in a small-angle X-ray scattering configuration is demonstrated using heterodyne techniques. Two examples are presented: the Brownian motion of latex spheres in glycerol, and a Doppler velocity experiment demonstrating the motion and the relaxation of carbon-black-filled elastomers after uniaxial stretching. In the latter case the effects of mechanical relaxation can be separated from those of aggregate diffusion. The results suggest that the dynamics of these filled elastomers are similar to the universal features observed in disordered jammed systems.

Keywords: coherent X-ray beams; dynamics of rubbers; heterodyne; small angles; speckles.

1. Introduction

Over the last several years the use of X-ray intensity fluctuation spectroscopy (XIFS) has been shown to be a useful technique for studying fluctuations in condensed matter systems. It provides a tool complementary to light scattering for the observation of small-scale high-q dynamics (see *e.g.* references 9–18 of Falus *et al.*, 2004). Even for length scales accessible to light scattering, it can be used for opaque samples or where multiple scattering impairs measurements.

For intensity fluctuation spectroscopy (IFS) with visible light, the signal-to-noise ratio can be increased by using heterodyne techniques. Heterodyne measurements require mixing in a reference signal, typically a fraction of the incident beam, which can easily be overlapped with the scattered beam using simple optics. Employing a reference signal also opens the possibility of obtaining phase information. Unfortunately the lack of suitable X-ray optics makes using a fraction of the incident beam for a reference signal difficult. This method was nevertheless used by Eisebitt *et al.* (2003) for soft X-rays by splitting the X-ray coherent beam transversally by means of a small aperture. X-ray heterodyning has also been reported by Gutt *et al.* (2003), where the reference signal was obtained through a fortuitous overlap of the specular and diffuse reflected scattering. More recently, heterodyning has been observed by interferences between fluctuating and non-fluctuating amplitudes in smectic membranes (de Jeu *et al.*, 2005).

In this paper we show that, by simply using a static random scatterer, heterodyning with X-rays can be performed in a controlled way in a small-angle configuration. We demonstrate the technique by studying the Brownian motion of latex spheres in glycerol and also by performing velocity measurements in a model rubber system of ethylene–propylene elastomers filled with carbon-black particles.

2. Description of the experiment

The experiments were carried out at the IMMY/XOR-CAT (8-ID) beamline at APS (Argonne, IL, USA) (Lumma *et al.*, 2000). This beamline used flat unfocusing optics. The monochromator was a Ge(111) channel-cut single crystal. The 15 μm × 15 μm beam size was selected by means of carefully polished slits placed 0.64 m before the sample. Guard slits were added, 0.16 m before the sample, in order to limit the scattering from slit diffraction in the SAXS region. The sample-to-detector distance was 2.8 m. A direct-illumination deep-depletion CCD (PI 1152 × 1242, 22.5 μm resolution) was used as an area detector. For the Ge(111) Bragg scattering, the energy resolution was $\delta\lambda/\lambda = 3.2 \times 10^{-4}$ and the longitudinal coherence length at the wavelength $\lambda = 1.62$ Å of the measurements was

$$\Lambda_1 = \lambda^2/2\delta\lambda = 0.25\,\mu\text{m}. \quad (1)$$

In our experiments, $2\theta < 10^{-2}$ rad, so that the wave pathlength difference ($2e\theta^2$) was less than Λ_1 for sample thickness e less than 5 mm. The total thickness of material in the scattering volume was kept below 2 mm, and interferences from scattering in this volume could be observed. The incident beam intensity was approximately 10^9 photons s^{-1}.

A heterodyne signal was obtained from a compacted powder of fume silica (Aerosil 200), 1 mm-thick, placed immediately upstream of the sample. The requirement for this reference sample is that it should occupy the same coherence volume as the specimen to be investigated. The resulting

combination of reference and dynamic sample is referred to as the hybrid sample. Aerosil provides a stable and strong X-ray scatterer covering a wide range of wavevectors. The sample holder was mounted on an x–z stage, perpendicular to the beam. By translating the sample holder, measurements could be made either directly on the fluctuating sample alone or on the hybrid sample, thus allowing for an easy comparison of homodyne and heterodyne results. In the latter case the beam intensity was reduced by a factor of 12 owing to the absorption in the reference.

3. Homodyne and heterodyne correlations

IFS allows a direct measure of the fluctuations in a sample. The expression for the time correlation function of the scattered amplitude $A_s(\mathbf{q}, t)$ (which depends on wavevector and time) from a sample is

$$G(\mathbf{q}, t) = \langle A_s(t') A_s^*(t' + t)\rangle_{t'} = \langle I_s(t)\rangle_t \gamma g_1(\mathbf{q}, t), \qquad (2)$$

where $\langle I_s(t)\rangle_t$ is a time average of the scattered intensity at wavevector $\mathbf{q}$. Partial coherence is taken into account by γ, and $g_1(\mathbf{q}, t)$ contains the sample dynamics $[g_1(\mathbf{q}, t = 0) = 1]$. For clarity, explicit wavevector dependence is omitted in A_s and I_s.

The (unnormalized) homodyne (G_1) intensity correlation function using (2) is

$$G_1(\mathbf{q}, t) = \langle I_s(\mathbf{q}, t)\rangle_t^2\big[1 + \beta|g_1(\mathbf{q}, t)|^2\big], \qquad (3)$$

where we have defined the 'zero time intercept', or the coherence factor, as $\beta = |\gamma|^2$. The set-up used in this experiment has been chosen in order that the overall coherence factor of the detected scattering intensity is $\beta \simeq 0.35$. This is a relatively large value for an XIFS experiment. Here we try to improve the signal-to-noise ratio and to limit sample irradiation. This estimate of β takes into account only transverse coherence (source, beam size, detection), as longitudinal coherence effects can be neglected with our monochromatic beam. This was verified by checking that β is almost independent of the diffraction angle θ in all our results. For heterodyning with a static reference signal $I_r(\mathbf{q})$ and a fluctuating sample signal I_s the correlation function (G_2) becomes (Geissler, 1993)

$$G_2(\mathbf{q}, t) = I_r^2 + \langle I_s(t)\rangle_t^2\big[1 + \beta|g_1(t)|^2\big] + 2I_r\langle I_s(t)\rangle_t + 2I_r\langle I_s(t)\rangle_t \beta\,\mathrm{Re}\big[g_1(t)\big]. \qquad (4)$$

This equation includes first- and second-order terms in the sample scattering intensity I_s, and we have assumed the same γ for homodyne and heterodyne measurements. Since the reference signal comes from a static disordered sample, averages over time and averages over wavevectors behave differently. This treatment extends equation (4) of László *et al.* (2003), which demonstrates heterodyning from the static parts of a gel. We restrict averages to a region of wavevectors Δ. The degree of mixing is defined as

$$x_\Delta = \langle\langle I_s\rangle_t\rangle_{\mathbf{q}\in\Delta}/\big(\langle I_r + \langle I_s\rangle_t\rangle_{\mathbf{q}\in\Delta}\big). \qquad (5)$$

x_Δ may depend on the region Δ. The domain Δ is chosen as a region where the scattering and correlation functions may be considered constant. For isotropic scattering, the domains are defined as rings: $|\mathbf{q}| \in (q - \delta q/2, q + \delta q/2)$. In our case the intervals Δq increase geometrically ($\delta q/q$ = a constant) because the SAXS intensity decreases more slowly for larger q values, and this improves the statistics for low counting rates. We now use the average $\langle \ldots \rangle_q$ to mean averages over $\mathbf{q}$ in Δ.

For $t \to 0$, equation (4) gives $\langle I_r + \langle I_s(t)\rangle_t\rangle_q^2(1 + \beta)$, and as $t \to \infty$ it becomes

$$\langle I_r + \langle I_s(t)\rangle_t\rangle_q^2\big[1 + \beta(1 - x)^2\big] = \langle\big[I_r + \langle I_s(t)\rangle_t\big]^2\rangle_q. \qquad (6)$$

This provides two different methods for normalizing the correlation functions. In one case we divide by $\langle I_r + \langle I_s(t)\rangle_t\rangle_q^2$, and the decay starts at $1 + \beta$. In the other, dividing by $\langle[I_r + \langle I_s(t)\rangle_t]^2\rangle_q$ makes the correlation function decay to unity. In either case the correlation function decays with an initial amplitude that is a fraction of β because the fluctuating signal is only a fraction of the total signal.

In the same experiment intensities can vary by several orders of magnitude. A droplet algorithm (Livet *et al.*, 2000) was used that transforms the CCD into a photon-counting area detector. This procedure optimizes experiments involving low intensities and a large number of frames and pixels. On applying this algorithm to all of our experiments, even where intensity is not too low, we also obtain a good estimate of the error bars in the correlation functions.

4. Dynamics of latex spheres in glycerol

As a first comparison of homodyne and heterodyne measurements, a suspension of latex spheres of diameter 98 nm in glycerol was studied. The suspension was contained in a 1 mm-diameter quartz capillary next to the reference. The sample was held at a constant temperature of 283 K, and the nominal latex volume fraction was 10%. As this system has a short fluctuation time, the CCD was divided into 18 strips, each of 64 rows, using the kinetics mode (Lumma *et al.*, 2000). The slits limited the exposed region of the CCD to about 900 × 54 pixels (horizontal × vertical). Data were recorded for strip exposure times of 25, 150, 350 and 1000 ms. The total exposure time was 30 s.

Fig. 1 compares the averaged cross sections of the aerosil alone, of the latex sample alone and of the hybrid sample. Intensities are corrected for absorption differences, monitor counts and measuring times. Clearly the latex sample has a strongly oscillating SAXS intensity, due to the form factor of the latex spheres. In the region where the scattering from the latex sample has a local minimum, intensities are obviously not constant, but these are so low that no result could be obtained for $q > 7 \times 10^{-3}$ Å^{-1}. The ratio x defined in (5) is always smaller than 0.1.

The top four curves of Fig. 2 show the normalized correlations $\langle G_1(t)\rangle_q/\langle\langle I_s(t)\rangle_t^2\rangle_q$ obtained for various values of t and q. The solid lines in this figure are the fits of the equation

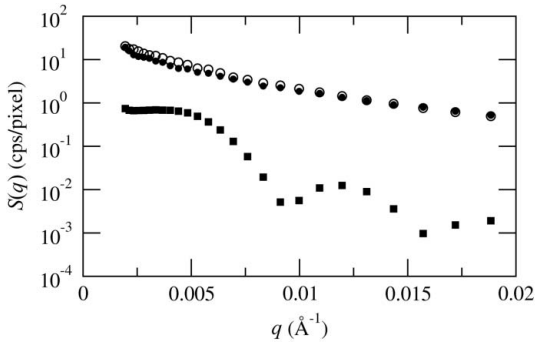

Figure 1
Isotropically averaged cross sections, normalized to compare the hybrid sample (aerosil + latex: open circles) count rate (in photons s^{-1} $pixel^{-1}$ for a 1×10^9 photons s^{-1} beam intensity) with the latex sample (closed squares) and the aerosil (closed circles).

$$\langle G_1(t)\rangle_q / \langle\langle I_s(t)\rangle_t^2\rangle_q = \{1 + \beta \exp[-2t/\tau_1(q)]\} \qquad (7)$$

to the normalized correlation functions. This exponential fit is in good agreement with our results. The fitted values of β lie between 0.33 and 0.36.

Typical heterodyne results, taken under identical conditions, are shown in the four lower plots of Fig. 2. In this case we calculate the correlation function $\langle G_2(\mathbf{q}, t)\rangle$, defined in (4), normalized by the value of (6), so that the result is unity for large values of t. As $x < 0.1$, the second-order terms in (4) can be neglected and accordingly the normalized correlations can be fit to the following simplified equation,

$$\langle G_2(t)\rangle_q / \langle [I_r + \langle I_s(t)\rangle_t]^2\rangle_q = \{1 + b \exp[-t/\tau_2(q)]\}, \qquad (8)$$

where $b \simeq 2x\beta/(1 + \beta)$. In the four lower curves of Fig. 2 it can be seen that the value of b increases with increasing q, reaches a maximum and then decreases. This is easy to relate to with the results of Fig. 1, where a maximum of $x \simeq 0.08$ occurs at $q \simeq 4 \times 10^{-3}$ Å^{-1}. This yields an estimate of the maximum of $b \simeq 0.04$, as observed in Fig. 2. It is clear that simply varying the thickness of the reference controls the amount of mixing.

We recall that, using the alternative normalization procedure, the correlation functions would start at $1 + \beta$ and decay to $[1 + \beta(1 - x)]$. The diffraction patterns have the same coherence as for homodyne measurements, but do not decay to 1.0 since only a fraction of the signal fluctuates.

These results provide a simple and direct comparison between the heterodyne and homodyne techniques. The physics of latex in glycerol is well described by Lumma *et al.* (2000) and we do not address it here. For the volume fraction studied here, the correlation functions are simple exponentials. Comparing $\tau_1(q)$ and $\tau_2(q)$ shows that the homodyne and heterodyne estimates are in agreement, as assured by the factor of 2 in (7), if the error bars of the fits are taken into account.

We may also compare the precision of the results shown in Fig. 2. In all cases independent data were assumed in fitting. Neglecting error cross-correlation in our data seems reasonable because the time series in each frame of the kinetic mode is short (only 15 strips were used) and the error bars increase

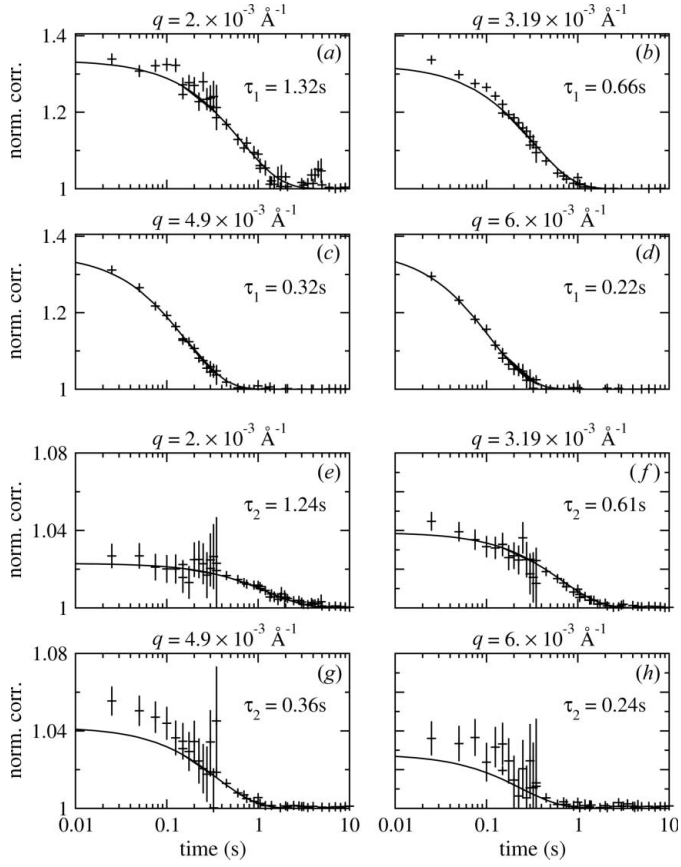

Figure 2
Homodyne (*a–d*) and heterodyne (*e–h*) correlations for latex spheres obtained for four q values. Correlations are plotted as a function of t. Error bars are calculated from formulae valid for small intensities. Fits corresponding to equation (8) are also shown, together with fluctuation times τ_1 and τ_2. Note that the last reliable result was obtained for $q = 6.7 \times 10^{-3}$ Å^{-1} and that $\tau_2 \simeq \tau_1$.

rapidly with the correlation time for the same series of frames. For the largest q, the ratio x becomes so small that the short time fluctuations are difficult to observe. In the intermediate range, for $q < 4 \times 10^{-3}$ Å^{-1}, the error bars for G_2 are less than twice those of G_1. This is best seen in Fig. 2 by comparing results for times greater than 0.3 s, which are obtained from the 150 ms exposure times. If one takes into account error bars from fitting and the factor of 2 in the homodyne correlation function, the heterodyne method gives roughly the same statistical error as the homodyne method. The intensity of the beam on the latex sample, however, is reduced by a factor of 12. This will be further discussed in another paper, but we note that it is advantageous for systems that are prone to radiation damage. Moreover, control of the relative scattering intensity is easily achieved by varying the thicknesses of the sample and of the reference.

5. Relaxation of filled polymers

As a second example, we use heterodyne measurements to study the microscopic relaxation of ethylene–propylene

rubbers (EPRs) filled with carbon black or fume silica (Ehrburger-Dolle *et al.*, 2003). The aim of the experiment was to compare relaxation mechanisms in cross-linked (CL-EPR) and uncross-linked (UCL-EPR) samples and to distinguish, during a relaxation process, between 'macroscopic' flow (the scale of the 15 µm pinhole) and 'microscopic' random fluctuations. These samples are either opaque to light (carbon black) or display strong multiple light scattering (silica), and they are also strong X-ray scatterers. Here we present data only on the carbon-black-filled samples (carbon-black volume fraction: 0.20). Samples were manually stretched by 100% in length, after which the strain was released, and alternating homodyne and heterodyne measurements were taken as the sample relaxed. The system was studied for times ranging from 1 min to a few hours after stretch.

Measurements were carried out using full CCD frames, with an exposure time of 0.25 s and a recurrence period of 3.95 s.

Fig. 3 shows the average cross section $S(q)$ measured with the hybrid sample. Units for this sample are counts s^{-1} $pixel^{-1}$, for a 10^9 photons s^{-1} beam intensity, which means that with a 0.25 s exposure time the counting rate per pixel varies from 5 to $\sim$0.02 in the q range of our measurement. In the same figure are plotted the corresponding cross sections of the reference and of the rubber, corrected for monitor intensities and sample transmission. It can be seen that the degree of mixing, x_Δ, is significantly larger here than for the latex case. Roughly speaking, x_Δ decreases from 0.5 to 0.1 in our q domain. For the very slow processes involved here, the limit $t = \infty$ is not easy to attain and it is more convenient to normalize $\langle G_2(\mathbf{q}, t)\rangle_q$ by $\langle I_r + \langle I_s\rangle_t\rangle_q^2$.

Owing to the relative velocity between the rubber and the aerosil, the correlation function acquires a phase factor of $\exp(i\mathbf{q}.\mathbf{v}t)$. We can define $\omega = \mathbf{q}.\mathbf{v} = qv\cos(\varphi)$. Heterodyning allows the effects of mechanical relaxation to be separated from the effects of diffusion of the filler particles. As the correlation function now depends on both $\cos(\varphi)$ and $|\mathbf{q}|$, the choice of the domains Δ must take account of the anisotropic character of the dynamics. For the discussion here, the domains Δ correspond to the same q domains as for the latex samples, but these domains must be subdivided into a set of values of $q\cos(\varphi)$. This means that the q domains are the intersection of a ring for a chosen set of $|\mathbf{q}|$ and a narrow band perpendicular to the direction of $\mathbf{v}$ for the selection of $q\cos(\varphi)$.

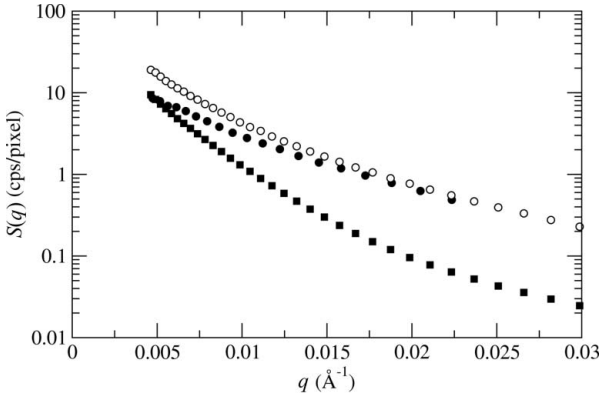

Figure 3
Isotropically averaged cross sections, normalized to compare the hybrid sample (aerosil + rubber: open circles) count rate (in photons s^{-1} $pixel^{-1}$ for a 1×10^9 photons s^{-1} beam intensity) with the rubber sample (closed squares) and the aerosil (closed circles).

Fig. 4 shows typical relaxations obtained from CL-EPR, 20000 s after release of stretching. These results were deduced from 500 frames, *i.e.* 125 s of measurement among roughly 2000 s of relaxation. The curves were obtained by averaging the heterodyne correlations over domains Δ centered on a value $|q_0|$ with $0.833q_0 < |\mathbf{q}| < 1.17q_0$. The angular domain ($\varphi$) had to be carefully selected. The symmetry constraint of changing φ to $180 - \varphi$ fixes the orientation of $\mathbf{v}$ with a precision of better than 0.2°. The direction of $\mathbf{v}$ was within 18° of the vertical axis, which is close to the direction of stretch. Although the correlation functions do not depend on the sign of $\mathbf{v}$, inspection of the speckle movement determines it unambiguously.

The four top curves (*a–d*) of Fig. 4 were obtained for the same $q_0 = 12 \times 10^{-3}$ Å^{-1} with four different values of $q\cos(\varphi)$ (0.57, 0.9, 1.21 and 1.52×10^{-3} Å^{-1}), and for a very narrow domain of variation $q\cos(\varphi)$ ($\pm 0.031 \times 10^{-3}$ Å^{-1}), in order to

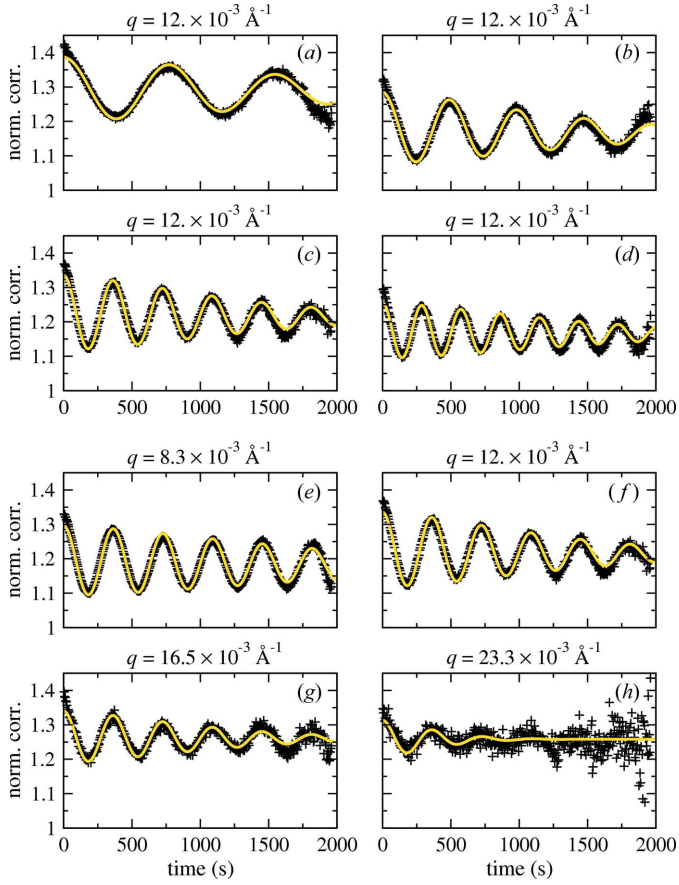

Figure 4
Heterodyne correlations obtained from the CL-EPR sample. (*a–d*) Various values of the $\mathbf{q}$ projections [$q\cos(\varphi) = 0.569$, 0.899, 1.21 and 1.52×10^{-3} Å^{-1}] along $\mathbf{v}$ for $q = 12 \times 10^{-3}$ Å^{-1}. (*e–h*) Various q values for $q\cos(\varphi) = 1.21 \times 10^{-3}$ Å^{-1} showing the identical period of the oscillations. Continuous curves correspond to fits with equation (9).

avoid mixing of oscillations of rapidly varying periodicities. A strong dependence of the oscillation periods upon $q\cos(\varphi)$ is observed.

The four lower curves (*e*–*h*) of Fig. 4 correspond to geometrically increasing values of q_0 (a factor close to $2^{1/2}$) for the same $q\cos(\varphi) = 1.21 \times 10^{-3}$ Å^{-1}. In this case the period of the oscillations remains the same, but their damping rates are different.

All fits of this figure use for the normalized correlation function the expression

$$g_2(q, \varphi, t) = 1 + \beta(1 - x)^2 + x^2\beta\gamma^2(t/\tau) + 2x(1 - x)\beta\cos(\omega t)\gamma(t/\tau). \quad (9)$$

This gives a fit with four parameters: β, x, ω and τ. The oscillation frequencies ω in (9) depend linearly on $|\mathbf{q}|$ and $\cos(\varphi)$. In Fig. 4 we observe that the period of the oscillations (*i.e.* ω) can be obtained with very good precision. We note in passing that the oscillations of the correlation functions, as seen in Fig. 4, are the Doppler shifts (Berne & Pecora, 2000) of the X-rays scattered from a material moving with a velocity of several Å s^{-1} [the result for Fig. 4 is 14.35 (2) Å s^{-1}].

The discussion on the damping term is somewhat more complex. We have chosen to fit using the equation $\gamma[t/\tau(q)] = \exp\{-[t/\tau(q)]^{1.5}\}$. This compressed exponential form is often preferred to a simple exponential in 'jammed' systems (Cipelletti *et al.*, 2003; Bandyopadhyay *et al.*, 2004). For the results of Fig. 4, only a small part of the detector is used, and the domains Δ contain between 100 and 400 pixels. The statistics are therefore insufficient to allow a detailed discussion of the various relaxation models. The same compressed exponential function was used for all φ, yielding the fitting curves plotted in Fig. 4.

In Fig. 5(*a*) the estimated values of ω are given at $q = 1.4 \times 10^{-2}$ Å^{-1} for different values of $\cos(\varphi)$. In Fig. 5(*b*), ω is plotted *versus* q for a fixed angle of 123°. The linear behavior of these curves provides a check of the expected **v.q** dependence.

Fig. 6 shows the relaxation velocities as a function of time for both cross-linked and uncross-linked samples. The relaxation of the velocities measured here (in our 15 µm × 15 µm area) agrees well in absolute value with macroscopic measurements of the shrinking of extended pieces of the same filled EPR rubber.

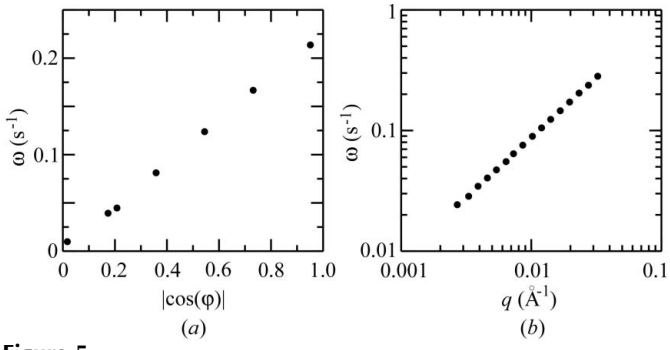

Figure 5
Calculated values of ω. (*a*) Various angles φ for $q = 1.4 \times 10^{-2}$ Å^{-1}. (*b*) Various q values for $\varphi = 123°$.

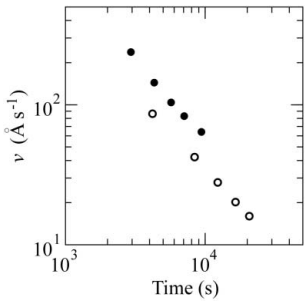

Figure 6
Relaxation of the velocities in both samples. The cross-linked specimen (open circles) is slower than the uncross-linked specimen (closed circles).

From the results of Fig. 4, rough estimates of τ can be given. For $q < 1 \times 10^{-2}$ Å^{-1}, results are widely scattered between 2500 s and 8000 s. These values are larger than the measuring time (2000 s for Fig. 4) and this means that damping is difficult to observe. For larger q, the fitted values of τ are decreasing with $|\mathbf{q}|$ and, for instance, the fits of the four lower curves (*e*–*h*) in Fig. 4 yield 2160 s, 1500 s, 1228 s and 480 s for τ. We also observe that the four top curves (*a*–*d*) of Fig. 4 should yield identical τ values: the results of the fits vary between 1500 s and 2100 s.

Further work is underway to understand the relationship between the correlation functions measured by homodyning and heterodyning in other similar systems.

6. Conclusion

We have shown that XIFS can be performed under controlled heterodyne conditions and this gives direct access to phase information. In particular, it is capable of measuring the phase shift in the scattering signal by the displacement of a sample with respect to a fixed reference. By its sensitivity to velocity distributions, useful insights should be obtained in systems that exhibit aging (Geissler *et al.*, 2000) or propagating waves (Gutt *et al.*, 2003). More generally, this type of measurement should be useful in systems in which viscoelastic effects are important, especially those displaying slow dynamics. It offers the possibility of discriminating between, at the scale of the X-ray beam (10 µm), semi-macroscopic flow from microscopic fluctuations in 'jamming systems'. Moreover, by virtue of the protection provided by a reference sample placed upstream, this type of measurement may be useful for limiting irradiation damage.

Use of the Advanced Photon Source was supported by the US Department of Energy, Office of Science, Office of Basic Energy Sciences, under Contract No. W-31-109-Eng-38.

References

Bandyopadhyay, R., Liang, D., Yardimci, H., Sessoms, D. A., Borthwick, M. A., Mochrie, S. G. J., Harden, J. L. & Leheny, R. L. (2004). *Phys. Rev. Lett.* **93**, 228302.

Berne, B. J. & Pecora, R. (2000). *Dynamic Light Scattering.* New York: Dover.
Cipelletti, L., Ramos, L., Manley, S., Pitard, E., Weitz, D. A., Pashkovski, E. E. & Johansson, M. (2003). *Faraday Discuss.* **123**, 237–251.
Ehrburger-Dolle, F., Bley, F., Geissler, E., Livet, F., Morfin, I. & Rochas, C. (2003). *Macromol. Symp.* **200**, 157–167.
Eisebitt, S., Lörgen, M., Eberhardt, W., Lüning, J., Stöhr, J., Rettner, C. T., Hellwig, O., Fullerton, E. E. & Denbeaux, G. (2003). *Phys. Rev. B*, **68**, 104419.
Falus, P., Borthwick, M. A. & Mochrie, S. G. J. (2004). *Rev. Sci. Instrum.* **75**, 4383–4400.
Geissler, E. (1993). *Dynamic Light Scattering*, edited by W. Brown, ch. 11. Oxford: Clarenden.
Geissler, E., Hecht, A. M., Rochas, C., Bley, F., Livet, F. & Sutton, M. (2000). *Phys. Rev. E*, **62**, 8308–8313.
Gutt, C., Ghaderi, T., Chamard, V., Madsen, A., Seydel, T., Tolan, M., Sprung, M., Grübel, G. & Sinha, S. K. (2003). *Phys. Rev. Lett.* **91**, 076104.
Jeu, W. H. de, Madsen, A., Sikharulidze, I. & Sprunt, S. (2005). *Physica B*, **357**, 39–44.
László, K., Kosik, K., Rochas, C. & Geissler, E. (2003). *Macromolecules*, **36**, 7771–7776.
Livet, F., Bley, F., Mainville, J., Caudron, R., Mochrie, S. G. J., Geissler, E., Dolino, G., Abernathy, D., Grübel, G. & Sutton, M. (2000). *Nucl. Instrum. Methods*, A**451**, 596–609.
Lumma, D., Lurio, L. B., Borthwick, M. A., Falus, P. & Mochrie, S. G. J. (2000). *Phys. Rev. E*, **62**, 8258–8269.